Nuclear Instruments and Methods in Physics Research B 568 (2025) 165869

Contents lists available at ScienceDirect

Nuclear Inst. and Methods in Physics Research, B

journal homepage: www.elsevier.com/locate/nimb

Efficient formation of negative ions for plutonium AMS☆

Michael Hotchkis [a,*], Keita Richardson [a], David Child [a], Dominik Koll [b], Anton Wallner [b], Klaus Wilcken [a]

[a] Centre for Accelerator Science, Australian Nuclear Science and Technology Organisation, New Illawarra Road, Lucas Heights, NSW 2234, Australia
[b] Accelerator Mass Spectrometry & Isotope Research, Helmholtz-Zentrum Dresden-Rossendorf, D-01328, Germany

ARTICLE INFO

Keywords:
Accelerator Mass Spectrometry
Actinides
Plutonium
Negative ions

ABSTRACT

In an Accelerator Mass Spectrometry (AMS) instrument, the detection efficiency for rare radioisotopes is determined by a combination of ionisation efficiency, charge state yield and beam transmission. Of these, ionisation efficiency remains as the principal limitation, with few instances where efficiency greater than 1 % has been reported. Using the Vega AMS system at ANSTO, we have achieved reproducible ionisation efficiency, for formation of PuO anions, of 3–4 %. However, the achievement of high overall efficiency has come at the cost of operational efficiency, as it can take at least 10 h to consume each sample.

We have performed a series of tests to understand what determines ionisation efficiency for plutonium AMS. In the standard method used at ANSTO, plutonium is dispersed in iron oxide and mixed with niobium as 'binder'. The overall efficiency for samples run to exhaustion is found to be linearly proportional to the total mass of loaded mixture. We have performed a series of tests investigating the effects of: (i) recess depth of material in the cathode; (ii) use of layered samples; (iii) binder / iron oxide mix; (iv) cathode materials; (v) different binder; (vi) sample surface area. We have also determined the molecular composition of the Pu anions: PuO_x^- of extracted beams for $x = 0$ to 3. The results are compared to a sputtering model that has been developed to account for the observed variation in count rates versus time as the sample is consumed. Ionisation efficiency up to 6.5 % has been observed for PuO anions.

1. Introduction

Accelerator Mass Spectrometry (AMS) is the method of choice for analysis of long-lived actinide radioisotopes when very high sensitivity is required. AMS has been used in recent studies where detection of very low abundance isotopes of uranium and plutonium provide key isotopic signatures to identify sources. Examples include detection of ^{233}U and ^{236}U in sediments and corals [1], $^{239-241}$Pu in soils and animal bones [2] and ^{244}Pu of extra-terrestrial origin [3]. In the latter study, ^{244}Pu of natural origin has been detected for the first time. The concentration of ^{244}Pu in a ferro-manganese crust from the Pacific Ocean was found to be $\sim 10^2$ atoms/g (~0.04ag/g), making it the rarest known naturally occurring radioisotope. Successful analyses of these rare radioisotopes depend on combining the low background inherent to AMS with high overall detection efficiency.

AMS systems generally use tandem accelerators and therefore require isotopes of interest to be injected as negative ions and converted to positive ions in the accelerator [4]. The efficiency of the AMS analysis system is determined by five factors: (i) the efficiency of formation of the negative ion used for analysis (referred to below as the ionisation efficiency), (ii) the yield of the charge state selected for analysis, (iii) the beam optic losses in the system, (iv) ion detection efficiency, and (v) the proportion of time spent analysing the radioisotope of interest. For AMS of actinides, the use of helium stripper gas in the terminal leads to 30–40 % yield to the 3+ charge state with terminal voltage in the range 0.25–1.0MV [5,6]. With careful design, the beam optic losses, including in the stripper, can be minimised [7]. Use of a simple ionisation chamber for actinides ensures close to 100 % detection efficiency. In AMS, isotopes of interest are analysed sequentially (not concurrently as in multi-collector mass spectrometers), so no isotope is analysed all the time. If there is only one very rare isotope of principal interest, then the timing can be adjusted to ensure that ~90 % of available time is spent on this isotope. These three factors lead to overall actinide detection efficiency, from ion source to detector, at around 25–30 % for a rare isotope.

☆ This article is part of a special issue entitled: 'Special Issue of AMS16' published in Nuclear Inst. and Methods in Physics Research, B.

* Corresponding author.
E-mail addresses: mah@ansto.gov.au, michael.hotchkis@physics.org (M. Hotchkis).

https://doi.org/10.1016/j.nimb.2025.165869
Received 29 May 2025; Received in revised form 3 September 2025; Accepted 12 September 2025
Available online 23 September 2025

The remaining factor to consider is the ionisation efficiency. In common with many forms of mass spectrometry, the principal limitation on the total detection efficiency of AMS is the ionisation efficiency. Atomic anions can be formed readily for elements with high electron affinity such as carbon, resulting in ionisation efficiency of around 5 % for ion sources used in AMS [4]. However, many metals have low electron affinity and do not form negative ions readily. Some, such as magnesium and zinc, have negative electron affinity and so the negative ions are unstable. Uranium has a low electron affinity (0.3 eV [8]), and the plutonium electron affinity is expected to be similar [9]. In such cases it has been shown that molecular anions have higher yields than the atomic anions [10], and in that paper Zhao et al. concluded that monoxide anions are the preferred option for uranium and plutonium.

Early research on actinides AMS used monoxide anions and the ionisation efficiencies for uranium and plutonium were estimated to be ~0.3 % and ~0.6 % respectively [11]. Fluorides of actinides have also been studied, as their use offers the potential for elemental selectivity [12]. Zhao and Francisco [13] have recently published a detailed study of polyatomic fluoride anions, with direct comparisons to oxides and hydroxides. Their paper also highlights the differing experiences of different AMS labs and the lack of clarity around the reasons for these differences.

In our recent work [6] using the Vega AMS facility at the ANSTO Centre for Accelerator Science, we have been able to demonstrate high overall efficiency of up to 1 %, corresponding to ~3 % ionisation efficiency when using PuO^- ions for analysis. This has been achieved by running samples to exhaustion, which can take 10–15 h. Hence high efficiency is achieved in a technical sense rather than an economic sense. However, for rare high value samples, such as deep-sea crusts [3,14], this approach is justifiable, and indeed is the only way of achieving the necessary sensitivity for successful detection of extra-terrestrial plutonium. Similar overall detection efficiencies have been reported by Christl et al. using the MILEA AMS [15].

The aim of the present work is to shed some light on factors that affect the ionisation efficiency and to find ways to improve it. There are many variables that are likely to impact on ion source performance and efficiency. In this work we have deliberately limited the scope, investigating effects related to the sample composition and geometry and cathode materials. An initial result, discussed in Section 3.1 below, demonstrated that the overall efficiency is correlated with the mass of material loaded in the sample cathode. This result raised several questions and motivated the experimental work that followed.

2. Methods

2.1. Cathode preparation

^{242}Pu-spiked iron oxide was prepared in ~200 mg quantities to allow many tests to be conducted using identical material. ^{242}Pu solution, prepared from NIST SRM 4334H, was combined with ferric nitrate solution (High Purity Standards, Cat: 1026 M-500) and coprecipitated. The precipitate was calcined to produce ^{242}Pu-spiked iron oxide powder as hematite (Fe_2O_3) [16], with concentration 50–300 fg ^{242}Pu/mg Fe. Calcination consists of ramping the temperature to 600 °C over a 4 h period, then holding the temperature for one hour, and cooling at a controlled rate. The calcined powder was ground to a fine powder and mixed with equal mass niobium powder using a mortar and pestle, in accordance with previous preparations [6]. The resulting material was used as our standard sample material, with which to test different geometries or to compare against variations of the sample material itself.

'Standard cathode' loading consisted of 10 mg standard sample material (as above, 5 mg ^{242}Pu spiked iron oxide +5 mg Nb) loaded into an aluminium (alloy-grade 2011-T3) NEC SNICS style cathode with sample diameter of 1.0 mm. An aluminium pin (1 mm diameter, length 0.5–1.0 mm) was placed behind the sample material and a pressure of 800 kPa was applied with a hydraulic press to compact the sample and pin. The depth of sample material is estimated to be 2.7 mm after compaction. Pressing was performed against a stainless steel pin such that the front of the sample was recessed by 0.5 mm from the front surface of the cathode. Every set of measurements performed contained at least one of these standard samples to serve as a reference, against which test cathodes were compared, allowing us to draw conclusions independent of variability in ion source and accelerator performance between runs.

Sample geometry test cathodes consisted of the following. Sample mass test cathodes were prepared exactly as for the standard cathode, but with differing amount of the identical sample material (^{242}Pu spiked iron oxide and Nb in equal parts) up to 13 mg total sample, the maximum that could be reliably loaded into an NEC standard cathode. Recess depth test cathodes were prepared as for the standard cathode but with 0.25 mm, 1.0 mm and 1.5 mm recess depths (in addition to 0.5 mm recess for the standard). To achieve this, sample material is pressed into the cathodes from the rear, against a projecting pin in the baseplate. Pins of different lengths are used to create the desired recess depth. In addition, conical pins were trialled, which produce a conical indent in the sample surface.

Furthermore, a set of layered test cathodes were prepared. These consisted of two types of sample material, the standard sample material, and a blank material which was prepared in the same way except that no Pu was included. Layering was achieved by loading material for the top layer into the cathode, applying direct pressure with the hydraulic press to create a defined layer boundary, and then loading the material for the bottom layer and pressing as per usual with the aluminium backing pin.

For material tests, cathodes were obtained fitting NEC specifications, but constituted of stainless steel (grade 316), copper (grade C101 99 % Cu), brass (grade 385C, ~58 % Cu, ~38 % Zn, ~4% Pb), magnesium (M3, 90 % Mg, ~6% Al, ~3% Zn), titanium (T2, 99 % Ti), and zinc (Z1, 99 % Zn). Binder material test cathodes were prepared with zinc powder as an alternative to niobium. For both Nb and Zn binders, binder ratio test cathodes were prepared with two or three times as much binder as ^{242}Pu-spiked iron oxide, while keeping the total mass of material (10 mg) consistent with our standard sample.

2.2. Vega AMS system operating conditions

The main purpose of the experiments described here was to test cathode configurations and sample composition. Therefore, as far as possible, all other variables were kept constant. Here we summarise the operating conditions and the beam tuning procedures that were used, noting that the experiments were conducted over a 2.5 year period involving multiple separate beam times. Details of the Vega AMS system can be found in Hotchkis et al. [6].

The ion source cathode voltage was set at 6.0 kV. This determines both the caesium sputtering beam energy and the initial acceleration of the negative ions. The caesium beam focus is determined by an immersion lens [17] and was set at a voltage of 5.2 kV. Importantly, this was not used as a tuning parameter and was never varied; the same setting was used during experiments where ionisation efficiencies were previously reported [6]. The beam is then accelerated by an extraction electrode set at 18 kV and focussed with an Einzel lens. The beam is further accelerated by the bias voltage, set at 46 kV, resulting in a total negative ion beam energy of 70 keV.

The ion source output was set to achieve a total negative ion output of ~ 100μA (dominated by O^- ions), with the current drawn by the cathode power supply generally in the range 1.0–1.2 mA (representing a combination of the Cs^+ beam, the negative ion beam and potentially some electron flow). The ioniser was set at ~200 W power and the caesium oven temperature was adjusted to achieve the above beam output. Ioniser and oven were manually adjusted within a narrow range during experiments to maintain the output. Steady ioniser power and Cs+ beam intensity ensures that the temperature reached by the cathode during sputtering is consistent for these test sample sets.

For the tests reported here, the Cs+ beam was always centred to within 0.2 mm, out of a sample diameter of 1 mm. It is our normal practice to adjust the wheel position after ion source servicing to centre it, and then to verify the centring after each sample wheel is removed from the source.

At the start of each run, a thorium-doped iron oxide sample (~1% Th) was used to generate a thorium beam for tuning, injecting a ThO^- and selecting $^{232}Th^{3+}$ after acceleration. The Einzel lens in the ion source was adjusted as part of the initial tuning procedure. The terminal voltage was set at 0.9MV and the helium gas stripper thickness was set to destroy molecules as previously described [6]. Using the thorium beam, all other system elements after the ion source were adjusted to optimise beam transmission through to the detector position. The beam transmission was measured with the thorium beam, generally achieving an accelerator transmission of around 33 % (3+ beam current after the first analyser divided by the injected ThO^- current). Beamline transmission was >90 %, using slit settings as typically used for routine actinides AMS analysis. The measured beam transmissions for each run were used to derive the ionisation efficiency (see below).

As previously described [6], following thorium beam tuning, the terminal voltage and electrostatic analyser were scaled to select plutonium isotopes, while all other beamline elements remained fixed. Using the high energy beam 'bouncers', with the terminal voltage and ESA at fixed values, the full range of plutonium isotopes were transmitted to the detector, all isotopes being measured within a cycle of around 1 s. Due to recent problems with the bouncer power supplies after the accelerator, some of the experiments described here were performed with a 'slow' cycling method, where the terminal voltage and electrostatic analyser were scaled for each isotope during a measurement cycle of around 100 s. For each experiment a set of plutonium isotopes were set up and checked with a plutonium standard. The standard was run periodically to check system stability. Generally, no re-tuning was performed for runs lasting several days, unless the isotope ratios of the standard were found to have drifted. In each ionisation efficiency experiment, multiple test cathodes were run, with samples being changed every 10–20 min, as would be done in AMS analysis runs.

2.3. Ionisation efficiency calculation

For results discussed in Section 3, the ionisation efficiency is calculated as the ratio of the detected ^{242}Pu atoms divided by the number of ^{242}Pu atoms in the sample, after applying known corrections for detection efficiency. This is done in the same way as previously [6] and is the same as described by Christl et al. [15]. The corrections include:

(i) Combined accelerator transmission and charge state yield as measured for the thorium beam; that is, Th^{3+} particle beam current after the first high-energy magnetic analyser divided by the injected ThO^- measured after the injection magnet.
(ii) Beamline transmission from the first high-energy analyser to the Faraday cup in front of the detector, as measured with the Th^{3+} beam.
(iii) Correction for time spent analysing isotopes other than ^{242}Pu and time spent switching between isotopes.

The efficiency calculations are subject to some assumptions and unknown factors:

(i) The charge state yield for plutonium is assumed to be the same as that measured for thorium. The charge state yields for uranium and thorium at around 1 MeV have been shown to be very similar [18]. We infer that other actinides may also be similar; however this cannot be proven in the absence of data for plutonium.
(ii) The extraction of negative ions from their point of production and their transmission to the point of injection into the accelerator is assumed to be 100 %, in the absence of any way of measuring this. The ion source and subsequent injection beamline are designed for full beam transmission; however, especially at high beam output, this is unlikely to be achieved. The calculated ionisation efficiencies therefore represent lower limits.

There are also some potential correction factors not included but known to be small, such as electronic deadtime, data transfer time and a short delay between sample insertion and the start of measurements. These factors were not always measured and have been treated as negligible here.

The maximum efficiency can only be achieved by running samples to exhaustion. As will be seen below, the count rate drops off exponentially in the later phase of sample consumption. For the purpose of this work, the sample is considered totally exhausted when the count rate has dropped below ~10 % of its peak count rate. At this point, at least 95 % of the sample has been consumed; when such cathodes are inspected post-run, there is no visible evidence of iron oxide in the cathode.

3. Results and discussion

3.1. Efficiency and sample mass

An initial observation in 2021 (see Fig. 1) demonstrated that the efficiency varies linearly with the mass of material loaded into the cathode. In this test, five different amounts of the same standard sample material, ranging from 3 to 13 mg, were loaded into cathodes and all were run to exhaustion. The test was repeated in 2022, with fresh material of different Pu concentration, ranging from 2 to 11 mg total mass. The ionization efficiency is seen to increase linearly with increasing sample mass, as opposed to the naive expectation that ionization efficiency should be constant regardless of sample mass. Specifically, this means that for iron oxide matrix with a given ^{242}Pu concentration, the total number of ^{242}Pu atoms detected had a quadratic dependence on the total number of ^{242}Pu atoms in the sample. Also, a number of samples which had been subjected to a full chemical extraction and purification procedure were analysed during this time period and run to exhaustion. All data are plotted in Fig. 1, showing that the dependence of efficiency on sample mass loaded is reproducible. Only processed samples with non-optimal yield fall off from this correlation. The preparation of the crust samples shown in Fig. 1 has been described by D. Koll [14,19].

To further illustrate the observed effect, the ^{242}Pu counting rate is plotted versus time in Fig. 2, during running of the 2022 sample set. Count rates rise over the course of the first hour of running; for high mass samples, the rate then reaches a plateau which is sustained for

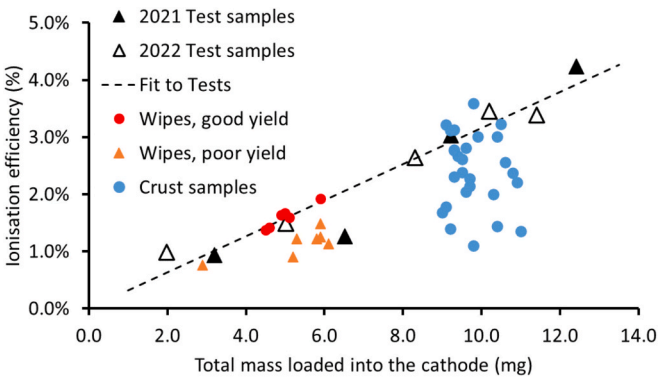

Fig. 1. Ionisation efficiency for PuO^- ions as a function of the total mass of sample material loaded into cathodes. Data include (i) two sets of ^{242}Pu spike test samples, run approximately a year apart in 2021 and 2022, (ii) two sets prepared from cotton wipes and (iii) a set of 27 samples each prepared from ~15 g of oceanic ferro-manganese crust material [19]. The dashed line is a linear fit to the two sets of Test samples (constrained to pass through the origin).

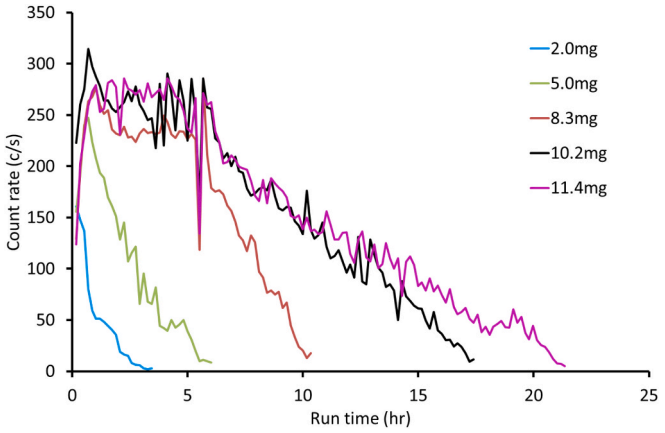

Fig. 2. Time dependence of ^{242}Pu count rates rate for different sample masses.

about 5 h before falling off in an extended tail stretching to many hours. For the smaller mass samples, the plateau is not attained and the counting rate drops off rapidly.

Samples with greater mass and therefore higher efficiency take longer to be sputtered to exhaustion, up to 20 h for the highest mass tests. This presents a practical difficulty for achieving the highest ionisation efficiencies for many samples on a regular basis. Due to the impracticality of long run times, detection efficiency achieved after 3 h, rather than after running to exhaustion, has been suggested as more relevant measure of performance [15]. By this metric, of the samples included in our mass test series, the 5.0 mg sample had the highest detection efficiency at 3hr, of 0.4 % (ionisation efficiency of 1.2 %).

3.2. Development of a sputtering model

We have developed a simple quantitative model of cathode sputtering to compare to observations.

3.2.1. Observations of sputtering geometry

Experimentally, we find that the rate of total mass sputtered is constant over the course of a run (Fig. 3). This was determined by measuring the mass of cathodes before and after sputtering for a range of times. The mass consumed is much greater than the amount of material loaded as the cathode itself and the backing pin are also sputtered. In addition, the crater depth for the same set of cathodes were measured (Fig. 3) by inserting a fine wire into the crater and measuring its length. The uncertainty was estimated to be ±0.2 mm.

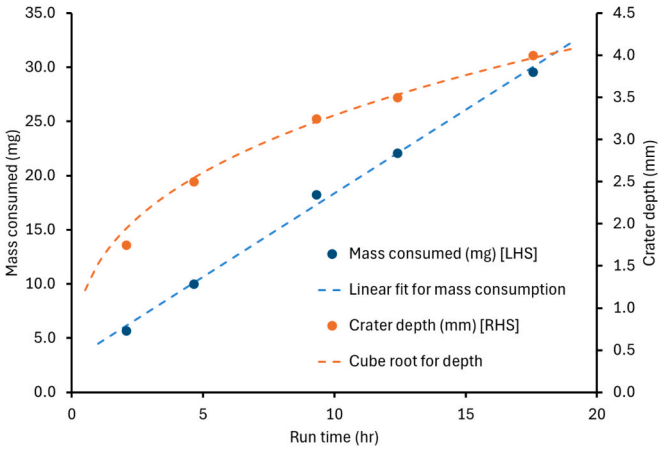

Fig. 3. Cathode mass (LHS) and crater depth (RHS) versus time, for standard reference samples (10 mg total mass) run for different times. The mass consumption is linear, while the depth matches a cube root function (see text).

3.2.2. Formulation of model

In our treatment of the cathode sputtering process, the shape of the sputtered crater is assumed to be a gaussian volume, and that the proportions of that gaussian are unchanged with time (depth is linearly related to full-width half-maximum). The choice of gaussian geometry is motivated by physical inspection of partially sputtered cathode craters (see Fig. 4), although in practice craters were often asymmetric or variable.

Given the observed constant sputtering rate by mass, and assuming a uniform density for the sputtered material, we can infer a constant rate of change of volume of our sputtered crater. Given also our earlier assumption that the proportions of our crater remain unchanged with time, that is that the crater volume is proportional to the linear dimension cubed, it can be shown that the linear dimension of our crater should grow in proportion to the cube root of the sputtering time, as observed in Fig. 3.

The expected count rate of an isotope uniformly distributed in the sample volume depends on (i) sample volume sputtered as a function of time and (ii) the ionisation probability. If it is assumed that the ionisation probability does not vary with time, then the maximum count rate should occur at the start of the run. The rate will then drop when sputtering of the surrounding cathode material begins, that is, when the sputter crater exceeds the dimensions of the cylindrical sample volume. This conflicts with the observed time dependence of the count rate (Fig. 2). Also, with an unvarying ionisation probability and complete consumption of sample material, the total ionisation efficiency would not be dependent on sample mass.

To explain the observed count rates and sputtering, it is necessary to introduce a time dependent factor to the ionisation probability. As a test, we hypothesize that the number of counts detected from the sputtering of a small volume of sample depends on the surface area of the sputtered crater at that time, that is, the amount of surface over which the incoming caesium beam is spread (inversely proportional to the flux of caesium).

The surface area A of the sputtered crater with depth a, width c, sample depth h is given by Eq. (1):

$$A = 2\sqrt{2}\pi c\left[x\sqrt{\ln\frac{a}{x}} - \frac{1}{2}\sqrt{\pi}\,a\,\mathrm{erf}\left(\sqrt{\ln\frac{a}{x}}\right)\right]_{ae^{\frac{-r^2}{2c^2}}}^{\min(a,h)} \quad (1)$$

The count rate was modelled as the rate of change of sample volume scaled by the area A of the crater surface area. As a further test, the count rate was modelled as scaling simply with the crater depth.

3.2.3. Model output

Fig. 5(a) shows the modelled count rate versus time with ionisation probability dependent on surface area and dependent on crater depth. We see a reasonable qualitative correspondence with experimental results from Fig. 2 in the count rate profile, where the initial increase, period of constant maximum, and then long tail of diminishing counts are all captured by the model, using either method of scaling. The initial increase in counts occurs as a result of starting with a small surface area of sample crater, which increases over time. This is moderated by the decreasing overlap of the sputter crater and the sample material as the run progresses. The region where the constant maximum counts occurs corresponds to where the sample crater surface area is increasing at a similar rate to the crater sample overlap decreasing. Eventually the

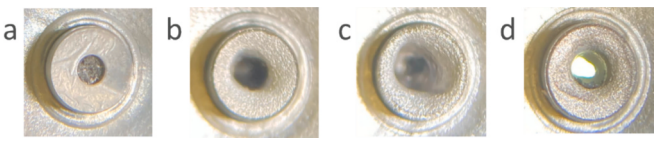

Fig. 4. Appearance of cathodes after sputtering for (a) 0 hr, (b) 4.7 hr (10 mg sample mass), (c) 17.6 hr (10 mg), (d) 3.4 hr (2 mg).

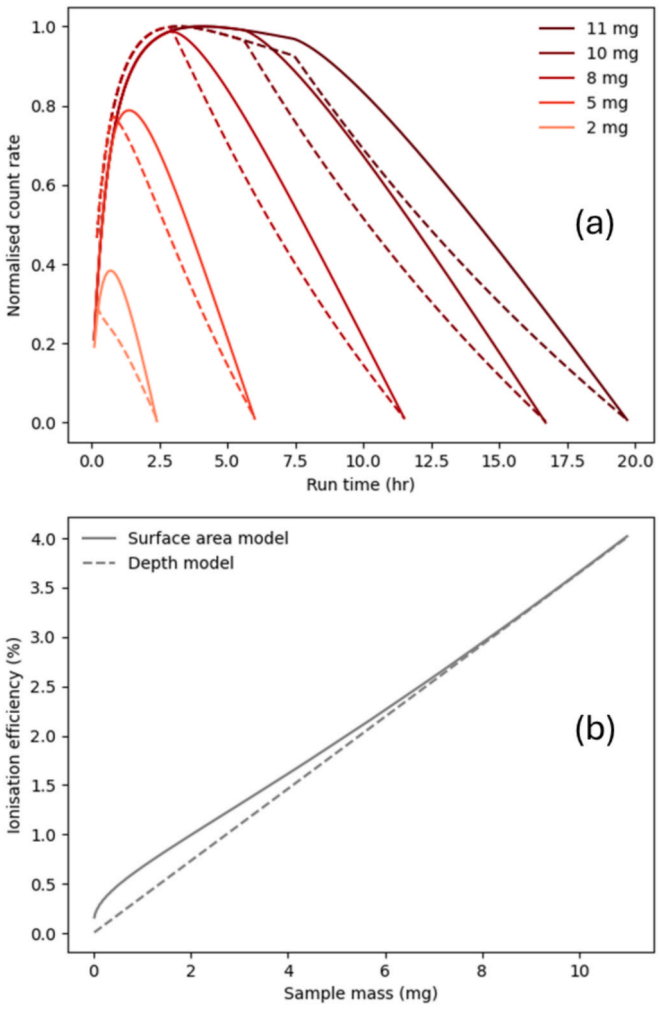

Fig. 5. (a) Modelled count rate versus time for five different total masses of material loaded; the solid lines indicate the modelled surface-area-dependent ionisation probability, with dashed lines for the depth-dependent version. (b) Efficiency versus sample mass for the two model versions.

overlap effect dominates and there is a long tail of decreasing count rate.

Importantly, the model also predicts (see Fig. 5(b)) a close to linear increase in ionisation efficiency versus sample mass for both model versions, similar to the experimental data in Fig. 1. This is because the higher mass samples are able to reach greater sample crater surface areas / greater crater depths over the course of their run.

3.3. Molecular composition

In our method the monoxide negative ions are selected for analysis. The observation of higher efficiency for higher sample mass indicates that the ionisation probability evolves as the sample is consumed. A possible reason for this could be that the molecular composition of the negative ion beam is evolving. Our use of monoxide ions is based on measurements of molecular composition of uranium and thorium anions at the time that AMS was first applied to actinides [10,20]. However, recent research has shown that the molecular composition for Pu may include significant amounts of dioxides and trioxides [13].

We have measured the molecular composition of Pu anions at different times during sample consumption. Three nominally identical 'baseline' cathodes were run for different times and then the anion composition was measured from each. The results are presented in Table 1. The monoxide is the dominant anion and this does not vary significantly during sample consumption. While this contrasts with the observations of Zhao and Francisco [13], it is noted the sample chemistry, the model of ion source and ion source operating conditions are all different between their work and ours.

Table 1
Pu anion composition of the beam at early, middle and late stage of sample consumption.

Sample ID	Run time (hr)	Pu^-	PuO^-	PuO_2^-	PuO_3^-
I6748	0.6	0.006 %	98.59 %	1.20 %	0.204 %
I6749	3.6	0.006 %	98.83 %	1.02 %	0.151 %
I6750	7.2	0.014 %	98.73 %	1.15 %	0.109 %
	Averages:	0.009 %	98.72 %	1.12 %	0.154 %

3.4. Sample geometry tests

3.4.1. Recess depth

A test was performed with a range of sample recess depths. Our standard cathode loading procedure produces samples which are recessed by 0.5 mm below the surface of the cathode, by pressing against a pin of length 0.5 mm. By using pins of different lengths, recesses of 0.25, 1.0 and 1.5 mm were produced. In one version of the model presented above, the ionisation probability is dependent on the sputtered crater depth; this test simply varies the depth at which the sample surface occurs to test if this affects ionisation probability. Alternatively, it could be hypothesized that a greater depth could produce greater opportunity for ionisation, as the greater surface area on the interior walls of the cathode could absorb neutrals, which could then be sputtered again with a further chance at ionisation. This is by analogy with the cavity filament used to enhance performance in thermal ionisation mass spectrometry (see for example Trinquier et al. [21]).

The 0.5, 1.0 and 1.5 mm recessed samples had ionisation efficiencies of 3.5 %, 3.7 %, and 3.6 % respectively. The 0.25 mm sample was not run to exhaustion but its count rate profile was similar to the others. Hence we conclude that there is no significant effect from recess depth.

3.4.2. Layered samples

For each interaction with a Cs cation, Pu atoms may have a significant probability of recoiling into the surface. A consequence of this would be the development of a concentration gradient of Pu through the column of sample material, resulting in increased counting rate as sputtering progresses. For samples with small mass, Pu atoms recoil into the aluminium backing pin earlier than for higher sample masses. Once embedded in aluminium, the ionisation probability is likely to be much diminished due to the absence of oxygen to form monoxide anions. Hence the overall ionisation efficiency would depend on sample mass.

To test this hypothesis, we prepared layered samples with standard sample material on top, and Pu-free blank material below, with total combined mass of 10 mg including binder. Pu recoils from the top layer can recoil into oxygen-containing blank material, hence are available for later ionisation. We may expect these layered cathodes to have efficiency greater than that from the same mass of spiked material loaded in the standard way.

The results from two test runs are shown in Table 2. Samples with a top layer of standard sample material on top of a layer of Pu-free blank material show some evidence of enhanced performance, in particular for the thinner top layers, lending support to the hypothesis. However, there is a significant amount of variability both within and between the tests. The reason for the generally poorer performances in Test 2 is not known.

3.4.3. Surface area test

A set of test samples were prepared, where the sample material was pressed against a conical pin, to create a conical indent in the sample surface. By using a conical pin with a 90° angle at its apex, the surface area was increased by $\sqrt{2}$. Using a 60° pin, the surface area was doubled. Two of each were run, along with 2 standard 'baseline' samples

Table 2
Results from layered samples. The relative enhancement factor is calculated from the efficiency of the 10 mg baseline sample measured in that test, assuming a linear dependence of efficiency on the mass of the spiked material loaded.

	Layer masses (mg)		Measured efficiency	Relative enhancement factor
	Top layer (242Pu spiked)	Bottom layer (unspiked)		
Test 1				
Baseline	10	–	3.75 %	–
2 mg normal	2	none	1.07 %	1.43
5 mg normal	5	none	1.62 %	0.86
1 mg layer test	1	9	1.06 %	2.83
2 mg layer test	2	8	1.33 %	1.77
3 mg layer test	3	7	1.60 %	1.42
Test 2				
Baseline	10	–	2.23 %	–
3 mg layer test	3	7	1.26 %	1.88
7 mg layer test	7	3	1.40 %	0.90

with flat surfaces.

The count rates for the first 4 h of running are shown in Fig. 6. It is clear that indentation makes no discernible difference in the time-dependence of the count rate, even from the start of running, when we would have expected the most effect from the surface area. The samples continued to run in a very similar way; after 13 h of running, the ionisation efficiencies of the six samples were in a narrow range between 4.9 and 5.4 %. This test shows that the surface area exposed to Cs beam is not a principal determinant of ionisation probability. Considering also the recess depth test in section 3.4.1, we conclude that there is another effect, so far not determined, which evolves with time in the same manner as the crater surface area or crater depth, which leads to increasing ionisation probability during sputtering.

3.5. Cathode and binder material tests

In addition to exploring the effects of cathode geometry on sputtering and ionisation efficiency, we have investigated the effects of using different materials, both in the cathode that holds the sample and in the binder. These materials may interact with the sample material and play a role in the formation of PuO anions, but since these interactions are poorly understood at a molecular level, we performed simple empirical tests comparing efficiency with different cathodes and binders.

3.5.1. Cathode effects

For many years we have used aluminium cathodes for plutonium AMS. Stainless steel and copper cathodes are routinely used for other AMS samples at our lab. An initial test in 2022 to compare aluminium with stainless steel and copper (Fig. 7) showed significant differences in ionisation probability and overall efficiency. We hypothesised that the efficiency of PuO anion formation might be influenced by the electron affinity of the material forming the cathode, with high electron affinity materials (such as copper) potentially competing for the electrons required for PuO^- formation. Therefore we tested several other cathode materials, specifically some with low or negative electron affinity. The ionisation efficiencies are shown in Fig. 7, at three stages of sample sputtering.

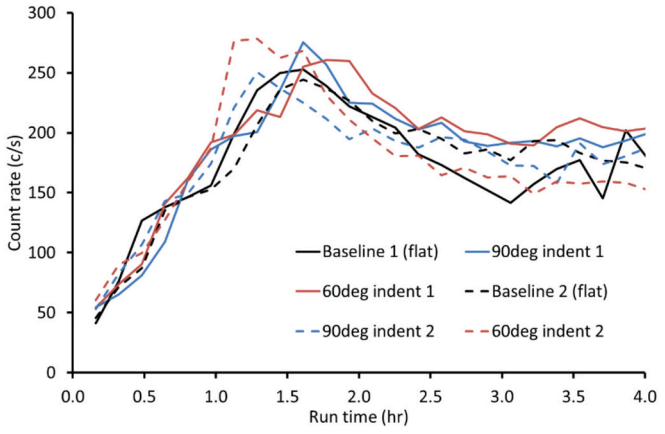

Fig. 6. ^{242}Pu count rates for samples with conical indents compared to standard flat-surfaced samples.

The material used in the cathode container clearly has a significant impact on plutonium ionisation efficiency. In the 2023 test run, efficiencies range from a lowest value of 3.1 % for the titanium cathode, up to a highest value of 6.6 % for magnesium. The stainless steel cathode tested in the same run also performed exceptionally well (6.3 % efficiency). A nickel cathode was run briefly in this run, but it was abandoned due to a very high count rate of interfering ions at mass 240, rendering it an impractical material for Pu analysis.

While those elements with negative electron affinity (Mg and Zn) performed well, Ti was the poorest despite its very low electron affinity, performing similarly to copper which has high electron affinity. So, the performance of cathodes is not found to correlate with the electron affinity of the material. The 2023 run is notable for the much higher efficiencies found for some materials, including standard aluminium cathodes, compared to other runs. It is possible that the presence of certain elemental materials on the cathode wheel led to a general enhancement of ionisation. Zinc in particular has a relatively high vapour pressure for a metal and may be responsible for this enhancement.

3.5.2. Binder effects

The effect of binder material on Pu ionisation efficiency was also tested. The standard cathode configuration consists of iron oxide mixed with niobium powder binder in equal parts by mass. It is expected that the binder improves electrical and thermal conductivity, allowing for charge dissipation from a sample being continually sputtered by positively charge Cs cations. Our earlier work [6] showed that niobium binder performed better than either silver binder or samples loaded without binder.

In two separate tests, the effect of binder proportion and binder material were tested, for niobium and zinc binders (see Fig. 8). In all test cathodes, 10 mg total mass of material (sample plus binder) was loaded, except in one case, where 8.5 mg was loaded (Zn 1:1 cathode in Binder Test B).

There is a significant difference between the overall ionisation efficiencies between the two tests, with test B giving much higher efficiencies in all cases. The reason for this difference is unclear. In Test B, the difference between the 1:1 and 2:1 Zn mixes can be attributed to the mass difference; if it is assumed that ionisation performance increases linearly with sample mass (as shown in section 3.1), then the 1:1 Zn has an estimated final efficiency of 6.50 % for a 10 mg total mass, not distinguishable from the 2:1 mix. Looking at the relative performance of

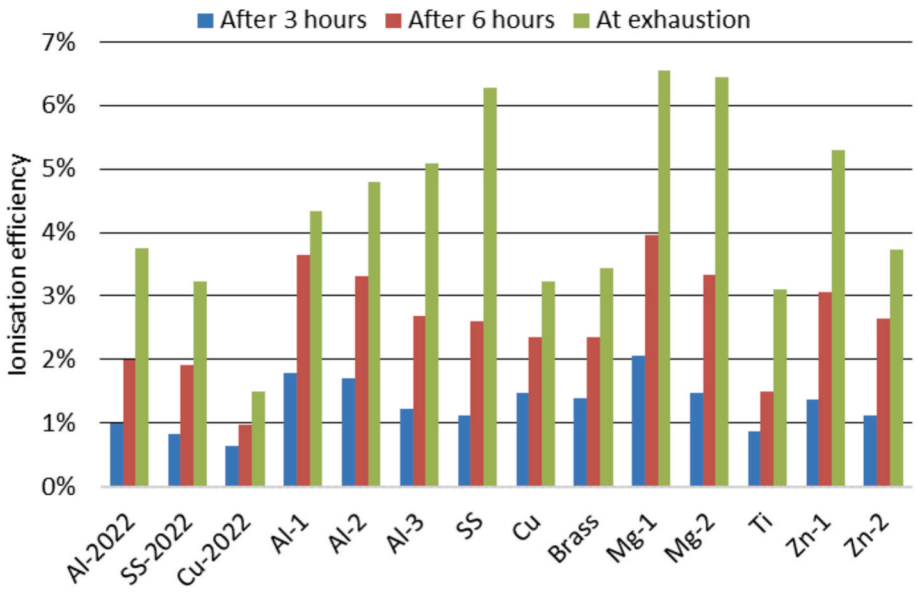

Fig. 7. Ionisation efficiencies for standard sample loading (10 mg total material) in cathodes made from different materials. Labels denote elemental or other cathode material (SS = stainless steel);'2022' denotes a test performed in 2022; all others were run together in a test in 2023. See section 2.1 for details of material grades used.

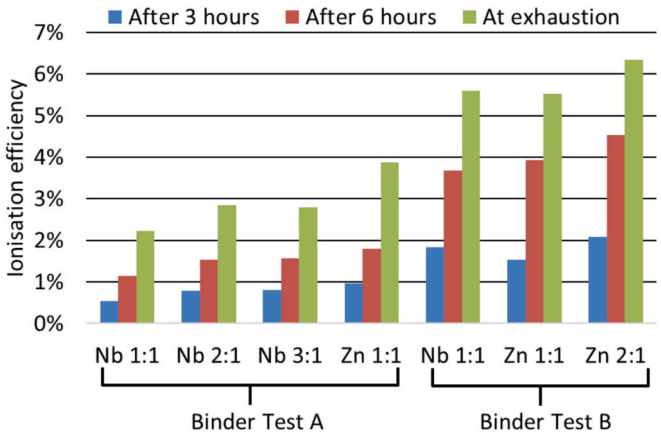

Fig. 8. Ionisation efficiencies for two binder test runs using niobium and zinc binders, including samples with differing proportions of binder.

the two binders, there is some indication that zinc binder enhances ionisation. There is also some indication that higher binder proportions in Test A outperformed the 1:1 mix.

4. Conclusions

The conclusions from the series of experiments we have carried out can be summarised as follows:

1. We have established a reproducible method for the achievement of overall detection efficiency in Pu AMS of greater than 1 %, corresponding to 3–4 % ionisation efficiency. This requires loading of ~10 mg of material in the cathodes and running the samples to near total exhaustion; this takes greater than 10 h per sample and so is usefully applicable only to high value samples.
2. A sputtering model has been developed which can account for the evolution of Pu ion count rate with time. The model needs to incorporate a factor whereby the ionisation probability increases during sample consumption. The physical origin of this factor has not been ascertained.
3. Tests have been conducted which indicated that the following parameters do not have a strong influence on ionisation probability: (i) sample recess depth in the cathode; (ii) initial surface area of the sample loaded in the cathode; (iii) binder:sample mass ratio.
4. Our operating conditions lead to a predominance (98 %) of plutonium anions as monoxide negative ions; this is highly favourable for efficient Pu AMS.
5. We observe significant variability between separate run times, despite attempting to reproduce identical running conditions. This demonstrates that there are factors significantly affecting ionisation probability that we have so far been unable to identify.
6. High ionisation efficiency, up to 6.5 %, has been achieved on a few occasions. The highest performance occurred during experiments where certain cathode or binder materials (zinc or magnesium) were present within the sample set. The cathode material has a strong influence on ionisation probability, for reasons that are not obvious. This in particular merits further attention.

CRediT authorship contribution statement

Michael Hotchkis: Writing – review & editing, Writing – original draft, Methodology, Investigation, Formal analysis, Data curation, Conceptualization. **Keita Richardson:** Writing – review & editing, Writing – original draft, Software, Methodology, Investigation, Formal analysis, Data curation, Conceptualization. **David Child:** Writing – review & editing, Methodology, Conceptualization. **Dominik Koll:** Writing – review & editing, Methodology, Formal analysis, Data curation, Conceptualization. **Anton Wallner:** Writing – review & editing, Conceptualization. **Klaus Wilcken:** Writing – review & editing, Methodology, Conceptualization.

Declaration of competing interest

The authors declare that they have no known competing financial interests or personal relationships that could have appeared to influence the work reported in this paper.

Acknowledgments

We acknowledge financial support from the Australian Government

for the Centre for Accelerator Science at ANSTO through the National Collaborative Research Infrastructure Strategy (NCRIS).

References

[1] K. Hain, P. Steier, M.B. Froehlich, R. Golser, X. Hou, J. Lachner, T. Nomura, J. Qiao, F. Quinto, A. Sakaguchi, 233U/236U signature allows to distinguish environmental emissions of civil nuclear industry from weapons fallout, Nat. Commun. 11 (2020), https://doi.org/10.1038/s41467-020-15008-2.

[2] M.P. Johansen, D. Anderson, D. Child, M.A.C. Hotchkis, H. Tsukada, K. Okuda, T. G. Hinton, Differentiating Fukushima and Nagasaki plutonium from global fallout using 241Pu/239Pu atom ratios: Pu vs, in: Cs Uptake and Dose to Biota, Science of the Total Environment 754, 2021, https://doi.org/10.1016/j.scitotenv.2020.141890.

[3] A. Wallner, M.B. Froehlich, M.A.C. Hotchkis, N. Kinoshita, M. Paul, M. Martschini, S. Pavetich, S.G. Tims, N. Kivel, D. Schumann, M. Honda, H. Matsuzaki, T. Yamagata, 60Fe and 244Pu deposited on Earth constrain the r-process yields of recent nearby supernovae, Science 372 (2021) (1979), https://doi.org/10.1126/science.aax3972.

[4] W. Kutschera, A.J.T. Jull, M. Paul, A. Wallner, Atom counting with accelerator mass spectrometry, Rev. Mod. Phys. 95 (2023), https://doi.org/10.1103/RevModPhys.95.035006.

[5] C. Vockenhuber, V. Alfimov, M. Christl, J. Lachner, T. Schulze-König, M. Suter, H. A. Synal, The potential of He stripping in heavy ion AMS, Nucl. Instrum. Methods Phys. Res. B 294 (2013) 382–386, https://doi.org/10.1016/j.nimb.2012.01.014.

[6] M.A.C. Hotchkis, D.P. Child, M.B. Froehlich, A. Wallner, K. Wilcken, M. Williams, Actinides AMS on the VEGA accelerator, Nucl. Instrum. Methods Phys. Res. B 438 (2019) 70–76, https://doi.org/10.1016/j.nimb.2018.07.029.

[7] M. Suter, S. Maxeiner, H.A. Synal, C. Vockenhuber, Charge-state distributions and charge-changing cross sections and their impact on the performance of AMS facilities, Nucl. Instrum. Methods Phys. Res. B 437 (2018) 116–122, https://doi.org/10.1016/j.nimb.2018.08.014.

[8] R. Tang, Y. Lu, H. Liu, C. Ning, Electron affinity of uranium and bound states of opposite parity in its anion, Phys. Rev. A (coll Park) 103 (2021), https://doi.org/10.1103/PhysRevA.103.L050801.

[9] M.-J. Nadeau, M.A. Garwan, X.-L. Zhao, A.E. Litherland, A negative ion survey; towards completion of the periodic table of the negative ions, Nucl. Instrum. Methods Phys. Res. B 123 (1997) 521.

[10] X.-L. Zhao, M.-J. Nadeau, M.A. Garwan, L.R. Kilius, A.E. Litherland, Radium, actinides, and their molecular negative ions from a cesium sputter ion source, Nucl. Instrum. Methods Phys. Res. B 92 (1994) 258–264.

[11] L.K. Fifield, Accelerator mass spectrometry of the actinides, Quat. Geochronol. 3 (2008) 276–290, https://doi.org/10.1016/j.quageo.2007.10.003.

[12] R.J. Cornett, Z.H. Kazi, X.L. Zhao, M.G. Chartrand, R.J. Charles, W.E. Kieser, Actinide measurements by AMS using fluoride matrices, Nucl. Instrum. Methods Phys. Res. B 361 (2015) 317–321, https://doi.org/10.1016/j.nimb.2015.02.039.

[13] X.-L. Zhao, B.B.A. Francisco, Matrix-assisted production of actinide molecular anions for AMS, Nucl. Instrum. Methods Phys. Res. B 510 (2022) 10–19, https://doi.org/10.1016/j.nimb.2021.10.013.

[14] D. Koll, A. Wallner, S. Battisson, S. Fichter, L.K. Fifield, M.B. Froehlich, J. Lachner, S. Merchel, S. Pavetich, G. Rugel, Z. Slavkovská, S.G. Tims, R. Ziegenrücker, Element separation chemistry and cosmogenic 10Be dating of a ferromanganese crust, Nucl. Instrum. Methods Phys. Res. B 530 (2022) 53–58, https://doi.org/10.1016/j.nimb.2022.08.017.

[15] M. Christl, P. Gautschi, S. Maxeiner, A.M. Müller, C. Vockenhuber, H.-A. Synal, 236U analyses with the ETH Zurich MILEA prototype system, Nucl. Instrum. Methods Phys. Res. B 534 (2023) 61–71, https://doi.org/10.1016/j.nimb.2022.11.009.

[16] D.P. Child, M.A.C. Hotchkis, K. Whittle, B. Zorko, Ionisation efficiency improvements for AMS measurement of actinides, Nucl. Instrum. Methods Phys. Res. B 268 (2010), https://doi.org/10.1016/j.nimb.2009.10.039.

[17] B.X. Han, J.R. Southon, M.L. Roberts, K.F. von Reden, Computer simulation of MC-SNICS for performance improvements, Nucl. Instrum. Methods Phys. Res. B 261 (2007) 588–593, https://doi.org/10.1016/j.nimb.2007.03.060.

[18] S.R. Winkler, P. Steier, J. Buchriegler, J. Lachner, J. Pitters, A. Priller, R. Golser, He stripping for AMS of 236U and other actinides using a 3 MV tandem accelerator, Nucl. Instrum. Methods Phys. Res. B 361 (2015) 458–464, https://doi.org/10.1016/j.nimb.2015.04.029.

[19] D. Koll, A 10-million year time profile of interstellar influx to Earth mapped through supernova 60Fe and r-process 244Pu, The Australian National University and Technical University Dresden, 2023.

[20] L.K. Fifield, R.G. Cresswell, M.L. di Tada, T.R. Ophel, J.P. Day, A.P. Clacher, S. J. King, N.D. Priest, Accelerator mass spectrometry of plutonium isotopes, Nucl. Instrum. Methods Phys. Res. B 117 (1996) 295–303, https://doi.org/10.1016/0168-583X(96)00287-X.

[21] A. Trinquier, C. Maden, A.-L. Fauré, A. Hubert, F. Pointurier, B. Bourdon, M. Schönbächler, More than five percent ionization efficiency by cavity source thermal ionization mass spectrometry for uranium subnanogram amounts, Anal. Chem. 91 (2019) 6190–6199, https://doi.org/10.1021/acs.analchem.9b00849.